

Symmetry Constraints and Variational Principles in Diffusion Quantum Monte Carlo Calculations of Excited-State Energies

W. M. C. Foulkes

Blackett Laboratory, Imperial College of Science, Technology and Medicine, Prince Consort Road, London SW7 2BZ, England

Randolph Q. Hood* and R. J. Needs

Cavendish Laboratory, Madingley Road, Cambridge CB3 0HE, England

(March 12, 2021)

Fixed-node diffusion Monte Carlo (DMC) is a stochastic algorithm for finding the lowest energy many-fermion wave function with the same nodal surface as a chosen trial function. It has proved itself among the most accurate methods available for calculating many-electron ground states, and is one of the few approaches that can be applied to systems large enough to act as realistic models of solids. In attempts to use fixed-node DMC for excited-state calculations, it has often been assumed that the DMC energy must be greater than or equal to the energy of the lowest exact eigenfunction with the same symmetry as the trial function. We show that this assumption is not justified unless the trial function transforms according to a one-dimensional irreducible representation of the symmetry group of the Hamiltonian. If the trial function transforms according to a multi-dimensional irreducible representation, corresponding to a degenerate energy level, the DMC energy may lie below the energy of the lowest eigenstate of that symmetry. Weaker variational bounds may then be obtained by choosing trial functions transforming according to one-dimensional irreducible representations of subgroups of the full symmetry group.

PACS: 71.10.-w, 71.15.Th, 02.70.Lq, 31.25.-v

I. INTRODUCTION

Quantum Monte Carlo (QMC) methods are powerful and general tools for calculating the ground-state electronic properties of atoms, molecules, and solids. Since the computational cost increases only as the cube of the number of particles, it is possible to study systems containing hundreds of electrons subject to periodic boundary conditions. This is enough to model real condensed matter with surprising precision, as shown by the accuracy of 0.1 eV per atom or better achieved in QMC calculations of the cohesive energies of solids. By comparison, the errors in local density functional calculations of cohesive energies are often of the order of 1 eV per atom.

The two most widely used QMC methods are variational Monte Carlo (VMC) and diffusion Monte Carlo (DMC).^{1,2} In VMC a trial many-electron wave function is chosen and expectation values are evaluated using Monte Carlo integration, which is more efficient than grid-based quadrature methods for high-dimensional integrals. Most VMC simulations of solids use trial wave functions containing a number of adjustable parameters, the values of which are determined by minimizing the energy or its variance.

DMC is a stochastic method for evolving a solution of the imaginary-time Schrödinger equation. The imaginary-time evolution gradually enhances the ground-state component of the solution relative to the excited-state components, but the algorithm does not maintain the fermionic symmetry of the starting state. The solution therefore converges towards the overall ground state, which is bosonic. This difficulty is known as the sign problem.

Although several exact solutions to the sign problem have been proposed, none has the statistical efficiency required to study the large systems of interest to condensed matter physicists. Most DMC simulations therefore use the approximate fixed-node method,³ which is numerically stable and often very accurate. The details will be described in Sec. II, but the basic idea is quite simple. A real trial many-electron wave function is chosen and used to define a trial nodal surface, which is the surface on which the trial function is zero and across which it changes sign. In a three-dimensional system containing N electrons, the trial wave function is a function of $3N$ variables, and the trial nodal surface is $3N - 1$ dimensional in general. The fixed-node DMC algorithm maintains the nodal surface of the trial wave function, so enforcing the fermionic symmetry and producing the lowest energy many-electron wave function consistent with that nodal surface.

Although VMC and DMC are principally ground-state methods, they can also provide some information about excited states. In particular, they can be used to study the lowest energy state of each distinct symmetry. In VMC this is done by choosing a trial wave function which possesses the required symmetry for all values of the variational parameters. The energy obtained after optimizing the trial function is therefore greater than or equal to the eigenvalue of the lowest energy eigenstate of that symmetry. A similar technique is also used in DMC, although this is much harder to justify. The problem is that the DMC trial function is only used to define the trial nodal surface, which may not be sufficient to fix the symmetry of the state produced by the stochastic DMC algorithm. In any case, practical tests have shown

that this approach often gives excellent results. Examples are the study of excitations of the hydrogen molecule by Grimes *et al.*,⁴ and calculations of excitation energies in diamond^{5,6} and silicon.⁷

If the trial function used in an excited-state DMC simulation has no definite symmetry, the only certainty is that the DMC energy must be greater than or equal to the many-electron ground-state energy.² In cases when the DMC trial function does have a definite symmetry, however, it is normally assumed that the fixed-node DMC solution has the same symmetry as the trial function, and hence that the DMC energy is greater than or equal to the eigenvalue of the lowest energy eigenstate of that symmetry. This symmetry-constrained variational principle is widely accepted, but we show by constructing a specific example that it is not always correct: the fixed-node DMC solution need not have the same symmetry as the trial function; and the fixed-node DMC energy may be lower than the energy of the lowest exact eigenstate of that symmetry.

The symmetry-constrained DMC variational principle is guaranteed to hold only when the trial function transforms according to a one-dimensional irreducible representation of the symmetry group of the Hamiltonian. The corresponding eigenstate is then non-degenerate, or has only accidental degeneracies. If the trial function transforms according to a multi-dimensional irreducible representation, corresponding to a degenerate energy level, the DMC energy may lie below the energy of the lowest eigenstate of that symmetry. In such cases a weaker variational principle may be obtained by choosing a trial function that transforms according to a one-dimensional irreducible representation of a subgroup of the full symmetry group. The DMC energy is then greater than or equal to the eigenvalue of the lowest exact eigenstate with that subgroup symmetry. This provides a strict variational lower bound for the DMC energy, but one that usually lies below the energy of the degenerate eigenstate of interest.

As an example, consider the case of a crystalline solid. Any trial function with a definite crystal momentum \mathbf{k} satisfies the many-electron version of Bloch's theorem and so transforms according to a one-dimensional irreducible representation of the translation group, which is a subgroup of the full symmetry group. The weaker variational principle therefore guarantees that the DMC energy must be greater than or equal to the energy of the lowest exact eigenstate with crystal momentum \mathbf{k} . Unfortunately, most Bloch states are complex and so cannot be used as fixed-node DMC trial functions. Real linear combinations of Bloch functions and their complex conjugates can be used instead, but in most cases these do not transform according to one-dimensional irreducible representations and do not lead to useful variational principles. This is illustrated in Sec. VIII, where we show that the DMC energy obtained using such a trial function may lie below the energy of the lowest eigenstate with crystal momentum \mathbf{k} .

The weaker variational principle is useful, but relies on a very careful choice of trial functions and cannot explain all the past successes of the fixed-node DMC method for excited states. The real explanation of these successes, we believe, is that although the DMC algorithm does not always preserve the symmetry of the trial function, the imposed nodal surface acts as such a strong restriction that the DMC solution cannot stray “too far” from that symmetry. The calculated energy is therefore close to the variational value that would have been obtained if the symmetry had been preserved. In cases when the excited state of interest satisfies the strong variational principle, the errors in the ground and excited state energies are guaranteed to have the same sign and tend to cancel, so improving the accuracy of the calculated energy difference.

The rest of this paper is organized as follows: Sec. II contains brief explanations of the DMC method and the fixed-node approximation for ground states; Sec. III shows that no general symmetry-constrained variational principle exists; Sec. IV shows that a variational theorem holds for the lowest energy state of each symmetry provided that the trial function transforms according to a one-dimensional irreducible representation of the group of spatial transformations of the Hamiltonian; Sec. V introduces a weaker variational principle which may give energy bounds even when the trial function transforms according to an irreducible representation of dimension greater than one; Sec. VI shows that a generalization of the tiling theorem⁸ holds in every case when we can prove that the DMC energy obeys a variational bound; Secs. VII and VIII give examples which demonstrate the absence of a general symmetry-constrained variational principle and illustrate the application of the weaker variational principle; and Sec. IX summarizes and concludes.

II. FIXED-NODE DIFFUSION MONTE CARLO FOR GROUND STATES

In this section we summarize the known results concerning the application of the fixed-node DMC method to ground states.^{1,2} The aim is to evaluate expectation values with an antisymmetric wave function $\Phi(X)$, where $X \equiv (x_1, x_2, \dots, x_N)$ lists the coordinates of all N electrons, and $x_i = (\mathbf{r}_i, s_{zi})$ specifies the position and spin projection of electron i . We choose wave functions with a fixed total $S_z = \sum_{i=1}^N s_{zi}$. The expectation value of a spin-independent symmetric operator $\hat{A}(\mathbf{R})$ is given by

$$\langle A \rangle = \frac{\sum_S \int \Phi^*(X) \hat{A}(\mathbf{R}) \Phi(X) d\mathbf{R}}{\sum_S \int \Phi^*(X) \Phi(X) d\mathbf{R}}, \quad (1)$$

where $\mathbf{R} \equiv (\mathbf{r}_1, \mathbf{r}_2, \dots, \mathbf{r}_N)$. For each spin configuration, S , the antisymmetric wave function $\Phi(X) = \Phi(x_1, x_2, \dots, x_N)$ may be replaced by a version with permuted arguments, $\Phi(x_{i_1}, x_{i_2}, \dots, x_{i_N})$, where the permutation is chosen such that the first N_\uparrow arguments are

spin-up and the last $N_\downarrow = N - N_\uparrow$ are spin-down. Since \mathbf{R} is a dummy variable, we can relabel $(\mathbf{r}_{i_1}, \mathbf{r}_{i_2}, \dots, \mathbf{r}_{i_N})$ as $(\mathbf{r}_1, \mathbf{r}_2, \dots, \mathbf{r}_N)$, after which the sums over spin configurations can be removed. The expectation value may then be written as

$$\langle A \rangle = \frac{\int \tilde{\Phi}^*(\mathbf{R}) \hat{A}(\mathbf{R}) \tilde{\Phi}(\mathbf{R}) d\mathbf{R}}{\int \tilde{\Phi}^*(\mathbf{R}) \tilde{\Phi}(\mathbf{R}) d\mathbf{R}}, \quad (2)$$

where

$$\tilde{\Phi}(\mathbf{r}_1, \mathbf{r}_2, \dots, \mathbf{r}_N) \equiv \Phi(\mathbf{r}_1, \uparrow; \mathbf{r}_2, \uparrow; \dots; \mathbf{r}_{N_\uparrow}, \uparrow; \mathbf{r}_{N_\uparrow+1}, \downarrow; \dots; \mathbf{r}_N, \downarrow). \quad (3)$$

The function $\tilde{\Phi}(\mathbf{r}_1, \dots, \mathbf{r}_N)$ is antisymmetric under interchange of any two of the up-spin arguments $\mathbf{r}_1, \dots, \mathbf{r}_{N_\uparrow}$ or any two of the down-spin arguments $\mathbf{r}_{N_\uparrow+1}, \dots, \mathbf{r}_{N_\uparrow+N_\downarrow}$, but has no definite symmetry under interchange of up- and down-spin arguments. It still obeys the Schrödinger equation, but the up- and down-spin electrons are now treated as distinguishable, allowing us to avoid explicit reference to the spin variables. For simplicity, all wave functions in the following discussion will be chosen to be of this type.

DMC is a method for solving the imaginary-time Schrödinger equation,

$$\left(-\frac{1}{2} \nabla_{\mathbf{R}}^2 + V(\mathbf{R}) - E_S \right) \Psi(\mathbf{R}, \tau) = -\frac{\partial}{\partial \tau} \Psi(\mathbf{R}, \tau), \quad (4)$$

where $\nabla_{\mathbf{R}}^2$ is shorthand for $\sum_{i=1}^N \nabla_i^2$. The potential $V(\mathbf{R})$ includes the electron-electron interactions as well as the external potential terms, and is assumed to be a local function of \mathbf{R} . It has Coulomb singularities whenever two charged particles approach each other, but is finite everywhere else. The constant energy shift E_S has been introduced to set a convenient zero of energy as explained below. The variable τ (which is real) is usually called the imaginary time, but we will often abbreviate “imaginary time” to “time” in what follows.

If the starting state $\Psi(\mathbf{R}, \tau = 0)$ is written as a linear combination of energy eigenfunctions,

$$\Psi(\mathbf{R}, \tau = 0) = \sum_i c_i \Psi_i(\mathbf{R}), \quad (5)$$

the large τ limit of the solution of Eq. (4) takes the form,

$$\Psi(\mathbf{R}, \tau \rightarrow \infty) = c_l \Psi_l(\mathbf{R}) e^{-(E_l - E_S)\tau}, \quad (6)$$

where $\Psi_l(\mathbf{R})$ is the lowest energy eigenfunction appearing in Eq. (5) and E_l is the corresponding eigenvalue. In applications to many-electron systems, $\Psi(\mathbf{R}, \tau = 0)$ is antisymmetric and $\Psi_l(\mathbf{R})$ is usually the many-electron ground state $\Psi_0(\mathbf{R})$. We will assume that the Hamiltonian \hat{H} is real (possesses time-reversal symmetry), in which case $\Psi_l(\mathbf{R})$ may also be chosen real and may be obtained by following the imaginary-time evolution of a real

function $\Psi(\mathbf{R}, \tau)$. If the Hamiltonian is complex (does not possess time-reversal symmetry), as when there is an applied magnetic field, the fixed-node DMC method discussed in this paper does not apply and it is necessary to use the fixed-phase method of Ortiz *et al.*⁹

DMC solves Eq. (4) using a stochastic algorithm, the efficiency of which is much improved by an importance sampling transformation.¹⁰ A real trial wave function $\Phi_T(\mathbf{R})$ is chosen and Eq. (4) is recast in terms of the product

$$f(\mathbf{R}, \tau) = \Psi(\mathbf{R}, \tau) \Phi_T(\mathbf{R}) \quad (7)$$

which is also real. After some straightforward algebra, $f(\mathbf{R}, \tau)$ is found to satisfy the equation,

$$-\frac{\partial}{\partial \tau} f(\mathbf{R}, \tau) = -\frac{1}{2} \nabla_{\mathbf{R}}^2 f(\mathbf{R}, \tau) + \nabla_{\mathbf{R}} \cdot [\mathbf{F}(\mathbf{R}) f(\mathbf{R}, \tau)] + (E_L(\mathbf{R}) - E_S) f(\mathbf{R}, \tau), \quad (8)$$

where $E_L(\mathbf{R}) \equiv \Phi_T^{-1}(\mathbf{R}) \hat{H} \Phi_T(\mathbf{R})$ is known as the local energy and $\mathbf{F}(\mathbf{R}) \equiv \Phi_T^{-1}(\mathbf{R}) \nabla_{\mathbf{R}} \Phi_T(\mathbf{R})$ as the quantum force. If the chosen trial wave function is close to the exact ground-state wave function, the local energy is nearly constant and the statistical efficiency of the algorithm is optimized.

If $f(\mathbf{R}, \tau)$ is constrained to be positive, Eq. (8) may be interpreted as describing the time evolution of the density of a population of “random walkers” multiplying or dying out as they diffuse and drift through a $3N$ -dimensional “configuration space”. The constraint that f is positive is known as the fixed-node approximation,³ because it forces the nodal surface of $\Psi(\mathbf{R}, \tau)$ to be the same as that of $\Phi_T(\mathbf{R})$. In practice, the distribution f is represented by a few hundred walkers propagating stochastically according to rules derived from Eq. (8). The growth or decay rate of the total number of walkers in the simulation depends on the average value of $E_L(\mathbf{R}) - E_S$, and the constant energy shift E_S is chosen to ensure that the population remains stable on average.

The initial walker positions are normally picked from the probability distribution $f(\mathbf{R}, \tau = 0) = (\Phi_T(\mathbf{R}))^2$, resulting in an initial population scattered throughout the configuration space. The nodal surface of $\Phi_T(\mathbf{R})$ divides this space into different nodal pockets, among which the walkers are distributed. During the simulation, the walkers never cross the fixed nodal surface separating one pocket from another, and so the fixed-node DMC algorithm proceeds independently in each pocket.

In the long-time limit, the probability density f of the walkers within nodal pocket v_α becomes proportional to $\phi_\alpha(\mathbf{R}) \Phi_T(\mathbf{R})$, where the “pocket ground state” $\phi_\alpha(\mathbf{R})$ is the lowest energy real normalized wave function which is zero outside v_α and satisfies the fixed-node boundary conditions on the surface of v_α . This function generally has gradient discontinuities across the surface of v_α , and the action of the kinetic energy operator on these discontinuities produces delta function terms which will be

denoted δ_α . The pocket ground state therefore satisfies the equations:

$$\left. \begin{aligned} \hat{H}\phi_\alpha(\mathbf{R}) &= \epsilon_\alpha\phi_\alpha(\mathbf{R}) + \delta_\alpha \\ \phi_\alpha(\mathbf{R})\Phi_T(\mathbf{R}) &\geq 0 \end{aligned} \right\} \quad \text{when } \mathbf{R} \in v_\alpha$$

$$\phi_\alpha(\mathbf{R}) = 0 \quad \text{when } \mathbf{R} \notin v_\alpha. \quad (9)$$

Since the walker density is positive, the sign of $\phi_\alpha(\mathbf{R})$ within v_α is the same as that of $\Phi_T(\mathbf{R})$, implying that $\phi_\alpha(\mathbf{R})$ and $\Phi_T(\mathbf{R})$ have a non-zero overlap. The form of $\phi_\alpha(\mathbf{R})$ does not depend on the details of $\Phi_T(\mathbf{R})$, but only on the shape of its nodal surface. The energy given by the DMC simulation in nodal pocket v_α is equal to the pocket eigenvalue ϵ_α . This need not equal the exact ground-state eigenvalue E_0 unless the trial nodal surface is the same as that of the exact ground state $\Psi_0(\mathbf{R})$, in which case $\phi_\alpha(\mathbf{R})$ is proportional to $\Psi_0(\mathbf{R})$ within v_α .

These results were used by Reynolds *et al.*¹⁰ and Moskowitz *et al.*¹¹ to prove that the fixed-node DMC energy is greater than or equal to the exact ground-state energy. Reynolds' proof starts from the solution in a single nodal pocket, and uses the permutations P that do not flip spins to construct a real wave function antisymmetric with respect to interchanges of electron coordinates of the same spin,

$$\bar{\Psi}_\alpha(\mathbf{R}) = \frac{1}{N_\uparrow!N_\downarrow!} \sum_P (-1)^P \phi_\alpha(P\mathbf{R}) \equiv \hat{A}\phi_\alpha(\mathbf{R}). \quad (10)$$

The function $\bar{\Psi}_\alpha(\mathbf{R})$ cannot equal zero everywhere since, at any point \mathbf{R} , all terms contributing to the sum in Eq. (10) have the same sign. This follows from the antisymmetry of the trial function $\Phi_T(\mathbf{R})$, which guarantees that all permutations P for which the point $P\mathbf{R}$ lies in nodal pocket v_α have the same parity (positive if the sign of the trial function at \mathbf{R} is the same as the sign of the trial function in v_α , negative otherwise). The function $\bar{\Psi}_\alpha(\mathbf{R})$ is however equal to zero everywhere on the trial nodal surface. This can be deduced from the knowledge that $\phi_\alpha(\mathbf{R})$ is equal to zero there (as well as in many other places), and that the nodal surfaces of antisymmetric functions such as $\Phi_T(\mathbf{R})$ are not altered by permutations.

The real antisymmetric function $\bar{\Psi}_\alpha(\mathbf{R})$ is now substituted into the standard quantum mechanical variational principle to give,

$$E_0 \leq \frac{\int \bar{\Psi}_\alpha \hat{H} \bar{\Psi}_\alpha d\mathbf{R}}{\int \bar{\Psi}_\alpha \bar{\Psi}_\alpha d\mathbf{R}} = \frac{\int \bar{\Psi}_\alpha \hat{H} \hat{A}\phi_\alpha d\mathbf{R}}{\int \bar{\Psi}_\alpha \hat{A}\phi_\alpha d\mathbf{R}}$$

$$= \frac{\int \bar{\Psi}_\alpha \hat{H} \phi_\alpha d\mathbf{R}}{\int \bar{\Psi}_\alpha \phi_\alpha d\mathbf{R}} = \epsilon_\alpha, \quad (11)$$

where we have used the fact that \hat{A} commutes with \hat{H} , that it is self-adjoint, and that it is idempotent (so that $\hat{A}\bar{\Psi}_\alpha(\mathbf{R}) = \bar{\Psi}_\alpha(\mathbf{R})$). The delta function terms appearing in $\hat{H}\phi_\alpha$ do not contribute to the energy expectation value because they occur on the fixed nodal surface where

$\bar{\Psi}_\alpha(\mathbf{R}) = 0$. If the nodal surface of $\Phi_T(\mathbf{R})$ is the same as the nodal surface of the exact ground state, the equality holds and the pocket eigenvalue ϵ_α is equal to E_0 ; but if $\Phi_T(\mathbf{R})$ does not have the correct nodal surface then $\epsilon_\alpha > E_0$. The energy ϵ_α produced by the DMC simulation in nodal pocket v_α is therefore minimized and equal to the exact ground-state energy when the trial nodal surface is exact. Since ϵ_α is also expected to depend smoothly on the shape of the nodal surface, it follows that the error in ϵ_α is in general second order in the error in the nodal surface.

For systems with reasonably well behaved local potentials and real ground-state wave functions, the tiling theorem⁸ states that all the ground-state nodal pockets are related by permutation symmetry. A derivation of this theorem appears in Sec. VI. The tiling theorem holds even when the ground state is degenerate, in which case every possible real linear combination of the degenerate ground states possesses the tiling property. Many DMC simulations use trial wave functions with the same nodal surface as the density-functional ground state. Since the density-functional Hamiltonian has a local potential, such trial states always satisfy the tiling theorem. This guarantees that the value of ϵ_α is the same in every nodal pocket, and hence that the energy obtained in the fixed-node DMC simulation cannot depend on how the walkers are distributed among the pockets.

In cases when the trial function does not possess the tiling property, the walker population grows most rapidly in nodal pockets with low values of ϵ_α (or, equivalently, low average values of $E_L(\mathbf{R}) - E_S$). Since E_S is chosen such that the total walker population stays roughly constant, and since fixed-node DMC walkers never cross from one nodal pocket into another, the walkers in less favorable pockets are gradually annihilated. Although many different nodal pockets may have contained walkers initially, the population becomes more and more concentrated in the pocket or pockets with the lowest value of ϵ_α , and it becomes more and more likely that only these pockets will be occupied. The DMC energy is therefore almost certain to converge to the lowest of the pocket eigenvalues of the nodal volumes initially occupied with walkers, $E_{\text{DMC}} = \min_\alpha(\epsilon_\alpha)$. This means that the energy obtained in a DMC simulation which does not possess the tiling property may depend on the initial distribution of walkers.

III. ABSENCE OF A GENERAL VARIATIONAL PRINCIPLE FOR FIXED-NODE DMC CALCULATIONS OF EXCITED STATES

In a few cases, the exact nodal surface of an excited-state wave function can be determined using symmetry arguments alone. An example is the first excited state of a particle in a one-dimensional square well, which has a single nodal point located at the well center. The trial wave function can then be chosen to have exactly the

same nodal surface as the excited state, and the fixed-node DMC simulation gives the exact excited-state eigenvalue. This result holds whether or not the trial wave function is orthogonal to all the lower energy eigenstates.

In practice, however, the exact nodal surface is rarely determined by symmetry alone, and it is rarely possible to choose a trial function with exactly the same nodal surface as the excited state of interest. Furthermore, the wave function of an arbitrary excited state need not possess the tiling property, and so the DMC energy may depend on the initial distribution of the walkers.

As an example, consider a hydrogen atom in its 2s state, $\Psi_{2s}(r)$, with eigenvalue E_{2s} . The exact nodal surface is a sphere of radius r_0 , the value of which cannot be determined using symmetry arguments. If the imposed nodal surface is exact, the pocket eigenvalues in the inner and outer pockets will both be exactly equal to E_{2s} ; but if the nodal surface is a sphere of radius $a \neq r_0$, the pocket eigenvalue $\epsilon_>$ of the wave function $\Psi_>$ in the outer pocket will not equal the pocket eigenvalue $\epsilon_<$ of the wave function $\Psi_<$ in the inner pocket.

Consider the case when the fixed node is too close to the nucleus, $a < r_0$. According to the variational principle applied to the outer pocket, the value of $\epsilon_>$ must be bounded above by the energy expectation value of the trial function,

$$\Phi_{\text{T}}^>(r) = \begin{cases} 0 & a \leq r \leq r_0 \\ \Psi_{2s}(r) & r > r_0 \end{cases} \quad (12)$$

This expectation value is the exact 2s eigenvalue E_{2s} . Clearly, we could construct a lower energy trial function by removing the kink in $\Phi_{\text{T}}^>(r)$ at $r = r_0$, and hence $\epsilon_> < E_{2s}$. Similarly, we can take the pocket ground state from the inner pocket, $\Psi_<$, and use it as a variational trial function within the exact 2s nodal surface $r = r_0$,

$$\Phi_{\text{T}}^<(r) = \begin{cases} \Psi_<(r) & r < a \\ 0 & a \leq r \leq r_0 \end{cases} \quad (13)$$

In this case the energy expectation value of the trial function is $\epsilon_<$, while the minimum possible expectation value for a wave function with a node at r_0 is E_{2s} . Again, we could construct a lower energy trial function by removing the kink at $r = a$, and hence $\epsilon_< > E_{2s}$. Note that variational arguments like these can be used whenever the exact nodal pocket completely encloses the trial pocket or vice-versa, irrespective of dimension or symmetry. This will prove useful in Sec. VIII.

The last paragraph showed that if $a < r_0$ then $\epsilon_> < E_{2s} < \epsilon_<$; if $a > r_0$, a similar derivation gives $\epsilon_< < E_{2s} < \epsilon_>$. The two pockets have different energies unless $a = r_0$. How does this affect the fixed-node DMC algorithm? As long as the lower energy pocket contains plenty of walkers initially, the walker population in the higher energy pocket will almost certainly die out. The fixed-node DMC energy will then tend to the pocket eigenvalue of the lower energy pocket, which is always less than or equal to E_{2s} . The DMC energy is therefore

maximized when $a = r_0$. If a is increased through r_0 , the $\tau \rightarrow \infty$ DMC walker population switches from the outer nodal pocket to the inner one, and the slope of the graph of the DMC energy versus a changes discontinuously. It follows that the error in the fixed-node DMC energy is first order in the error in the nodal surface, not second order as it is for the ground state. This example shows that there is no variational principle when fixed-node DMC is used to study general excited states: the error in the DMC energy of the excited state may increase linearly with the error in the nodal surface; and the DMC energy need not be minimized when the nodal surface is exact.

IV. THE LOWEST ENERGY EIGENSTATE OF EACH SYMMETRY

We now address the question of whether there is a variational principle for fixed-node DMC simulations of the lowest energy state of each symmetry. We denote by \mathcal{G} the group of spatial transformations \mathcal{T} (combinations of rotations, reflections, translations, and inversions of all electrons simultaneously) which leave the many-electron Hamiltonian invariant. For simplicity, we consider this group to be finite¹² and of order g . The full symmetry group of the Hamiltonian is the direct product of \mathcal{G} with the permutation and time-reversal groups. All the symmetry arguments in this paper can easily be recast in terms of the full symmetry group instead of \mathcal{G} , but real many-electron wave functions have such simple time-reversal and permutation symmetries (they transform according to the one-dimensional identity representation of the time-reversal group and the one-dimensional antisymmetric representation of the permutation group) that this is unnecessary. Since the arguments based on the spatial group \mathcal{G} are somewhat easier to grasp, we choose to work with this group in what follows.

We begin by showing that a symmetry-constrained variational principle holds whenever the chosen trial function is real and has an invariant nodal surface. This theorem was stated without proof in a paper by Caffarel and Claverie.¹³ Here we sketch a proof.

A real trial function $\Phi_{\text{T}}(\mathbf{R})$ is said to have an invariant nodal surface if the transformed function,

$$\hat{Q}(\mathcal{T})\Phi_{\text{T}}(\mathbf{R}) \equiv \Phi_{\text{T}}(\mathcal{T}^{-1}\mathbf{R}), \quad (14)$$

has the same nodal surface as $\Phi_{\text{T}}(\mathbf{R})$ for all coordinate transformations $\mathcal{T} \in \mathcal{G}$. Note that the nodal surface is defined as the surface on which $\Phi_{\text{T}}(\mathbf{R})$ is zero and across which it changes sign; $\Phi_{\text{T}}(\mathbf{R})$ may also have additional zeros where the sign does not change, but these are not on the nodal surface and need not be invariant.

The proof relies on the properties of the function $\chi(\mathbf{R})$ defined by,

$$\chi(\mathbf{R}) = \begin{cases} 0 & \text{on the trial nodal surface} \\ +1 & \text{in nodal pockets where } \Phi_T \geq 0 \\ -1 & \text{in nodal pockets where } \Phi_T \leq 0. \end{cases} \quad (15)$$

Given any point \mathbf{R} not on the nodal surface, and any spatial transformation $\mathcal{T} \in \mathcal{G}$, it is clear that $\chi(\mathbf{R}) = \eta\chi(\mathcal{T}^{-1}\mathbf{R})$, where $\eta = \pm 1$. Furthermore, since the functions $\chi(\mathbf{R})$ and $\chi(\mathcal{T}^{-1}\mathbf{R})$ have the same nodal surface and so change sign together as \mathbf{R} changes, the sign of η must be independent of \mathbf{R} . This shows that all symmetries $\mathcal{T} \in \mathcal{G}$ either leave $\chi(\mathbf{R})$ unchanged or multiply it by -1 , from which it follows that $\chi(\mathbf{R})$ transforms according to a one-dimensional irreducible representation $\Gamma_{\mathcal{G}}^r$ of \mathcal{G} .

We can now adapt the proof of the ground-state variational principle given in Sec. II. Take the pocket ground state ϕ_α and antisymmetrize it to obtain a function $\bar{\Psi}_\alpha$ as in Eq. (10). Now apply the group theoretical projection operator,¹⁴

$$\hat{\mathcal{P}}^r = \frac{1}{g} \sum_{\mathcal{T} \in \mathcal{G}} \Gamma_{\mathcal{G}}^r(\mathcal{T}) \hat{Q}(\mathcal{T}), \quad (16)$$

where $\Gamma_{\mathcal{G}}^r(\mathcal{T})$ is the one-by-one matrix representing \mathcal{T} . The application of $\hat{\mathcal{P}}^r$ produces a new antisymmetric state $\bar{\Psi}_\alpha^r$ which transforms according to the one-dimensional irreducible representation $\Gamma_{\mathcal{G}}^r$. Since the original pocket ground state $\phi_\alpha(\mathbf{R})$ had a non-zero overlap with $\chi(\mathbf{R})$, which is itself an antisymmetric function of symmetry $\Gamma_{\mathcal{G}}^r$, the antisymmetric $\Gamma_{\mathcal{G}}^r$ component projected out by applying $\hat{\mathcal{A}}$ and then $\hat{\mathcal{P}}^r$ to ϕ_α cannot be zero.

The energy expectation value of $\bar{\Psi}_\alpha^r$ is greater than or equal to the energy E_0^r of the lowest antisymmetric state of symmetry $\Gamma_{\mathcal{G}}^r$,

$$\begin{aligned} E_0^r &\leq \frac{\int \bar{\Psi}_\alpha^{r*} \hat{H} \bar{\Psi}_\alpha^r d\mathbf{R}}{\int \bar{\Psi}_\alpha^{r*} \bar{\Psi}_\alpha^r d\mathbf{R}} = \frac{\int \bar{\Psi}_\alpha^{r*} \hat{H} \hat{\mathcal{P}}^r \hat{\mathcal{A}} \phi_\alpha d\mathbf{R}}{\int \bar{\Psi}_\alpha^{r*} \hat{\mathcal{P}}^r \hat{\mathcal{A}} \phi_\alpha d\mathbf{R}} \\ &= \frac{\int \bar{\Psi}_\alpha^{r*} \hat{H} \phi_\alpha d\mathbf{R}}{\int \bar{\Psi}_\alpha^{r*} \phi_\alpha d\mathbf{R}} = \epsilon_\alpha. \end{aligned} \quad (17)$$

In analogy with the ground-state proof of Sec. II, these manipulations rely on the self-adjointness and idempotency of the operators $\hat{\mathcal{A}}$ and $\hat{\mathcal{P}}^r$, both of which commute with \hat{H} . It is also important that $\bar{\Psi}_\alpha^{r*}(\mathbf{R})$ is equal to zero everywhere on the surface of v_α , so that the delta function terms in the expression for $\hat{H}\phi_\alpha(\mathbf{R})$ from Eq. (9) do not contribute to the expectation value. This is guaranteed because the fixed nodal surface is invariant.

Note that the symmetry of the trial function played no part in this derivation; the only thing that mattered was the invariance of the trial nodal surface. In most DMC simulations, however, the trial function does have a definite symmetry, and so transforms according to a specific irreducible representation of \mathcal{G} . Given that functions transforming according to different irreducible representations are orthogonal, and that the definition of $\chi(\mathbf{R})$

ensures that $\langle \chi | \Phi_T \rangle > 0$, it follows that any trial function with a definite symmetry and an invariant nodal surface must transform according to the same one-dimensional irreducible representation as the corresponding $\chi(\mathbf{R})$. This implies that a real trial function transforming according to an irreducible representation of dimension greater than one cannot have an invariant nodal surface.

The converse is also true: any real trial function $\Phi_T(\mathbf{R})$ transforming according to a one-dimensional irreducible representation must have an invariant nodal surface. This follows from the transformation law,

$$\hat{Q}(\mathcal{T})\Phi_T(\mathbf{R}) = \Gamma_{\mathcal{G}}^r(\mathcal{T})\Phi_T(\mathbf{R}), \quad (18)$$

and the observation that the real normalized function $\Phi_T(\mathbf{R})$ remains real and normalized under all transformations in \mathcal{G} . The one-by-one matrix $\Gamma_{\mathcal{G}}^r(\mathcal{T})$ is therefore equal to ± 1 , and the nodal surface of $\hat{Q}(\mathcal{T})\Phi_T(\mathbf{R})$ is the same as that of $\Phi_T(\mathbf{R})$.

Putting everything together, we can now conclude that whenever the real trial function transforms according to a one-dimensional irreducible representation of \mathcal{G} , the nodal surface is invariant, and the DMC energy is greater than or equal to the energy of the lowest exact eigenfunction with that symmetry. This is the symmetry-constrained variational principle mentioned in the introduction. If the trial function transforms according to an irreducible representation of dimension greater than one, the nodal surface cannot be invariant, and the delta functions produced when \hat{H} is applied to ϕ_α need not all occur where $\bar{\Psi}_\alpha^{r*} = 0$. The above proof of the symmetry-constrained variational principle therefore breaks down. In Sec. VIII we give an example of a system with a trial function transforming according to an irreducible representation $\Gamma_{\mathcal{G}}^r$ of dimension $d_r = 2$ for which $E_{\text{DMC}} < E_0^r$.

The restriction of the variational principle to trial functions transforming according to one-dimensional irreducible representations can be understood in a very simple way. The problem being solved in a fixed-node DMC simulation is not the imaginary-time Schrödinger equation of Eq. (4), but the imaginary-time Schrödinger equation subject to the additional boundary conditions specified by the trial nodal surface. As a result, the relevant symmetry group is not the group \mathcal{G} of symmetries of \hat{H} , but the subgroup \mathcal{G}_{FN} that leaves both the Hamiltonian and the fixed nodal surface (boundary conditions) invariant. The fixed-node eigenfunctions need only conform to the symmetries in \mathcal{G}_{FN} , and their transformation properties should be analyzed in terms of the irreducible representations of \mathcal{G}_{FN} , not \mathcal{G} . If the real trial function transforms according to a one-dimensional irreducible representation of \mathcal{G} , the fixed nodal surface is invariant and the groups \mathcal{G} and \mathcal{G}_{FN} are the same. The symmetry-constrained variational principle discussed in this section does not apply unless this is the case.

V. IRREDUCIBLE REPRESENTATIONS OF DIMENSION GREATER THAN ONE

Can anything be said when the trial function transforms according to an irreducible representation of dimension greater than one? Suppose that the real trial function $\Phi_{T,l}^r(\mathbf{R})$ transforms as the l th row of an irreducible representation $\Gamma_{\mathcal{G}}^r$ with dimension $d_r > 1$. We already know that the nodal surface of $\Phi_{T,l}^r(\mathbf{R})$ cannot be invariant with respect to all the operations in \mathcal{G} , but it may be invariant under a subset of those operations. Any such subset forms a proper subgroup, \mathcal{G}_{FN} , which in general depends on the row index l .

As in Sec. IV, we define the function $\chi(\mathbf{R})$ which is equal to +1 in all nodal pockets where $\Phi_{T,l}^r(\mathbf{R}) \geq 0$, equal to -1 in all nodal pockets where $\Phi_{T,l}^r(\mathbf{R}) \leq 0$, and equal to zero everywhere on the nodal surface of $\Phi_{T,l}^r(\mathbf{R})$. By construction, $\chi(\mathbf{R})$ transforms according to a one-dimensional irreducible representation of \mathcal{G}_{FN} (although not of \mathcal{G}). Since all the pocket ground states ϕ_α have non-zero overlaps with $\chi(\mathbf{R})$, they all have non-zero components of the same subgroup symmetry as $\chi(\mathbf{R})$. We can therefore re-use the symmetry-projection argument leading to Eq. (17) to show that the fixed-node DMC energy is greater than or equal to the eigenvalue of the lowest energy exact eigenfunction with the same subgroup symmetry as $\chi(\mathbf{R})$. This provides a rigorous variational principle, but the subgroup \mathcal{G}_{FN} that leaves the trial nodal surface invariant is usually small and its irreducible representations provide a correspondingly limited set of symmetry labels. The bounds obtained are therefore weak and this variational principle is of little use unless optimized as explained below.

If the nodes of $\Phi_{T,l}^r(\mathbf{R})$ were exact one could form a trial function from any real linear combination of different rows and always obtain the same DMC energy. When the nodes are not exact, however, the DMC method breaks this d_r -fold degeneracy, and the variational lower bound on the DMC energy depends on the precise linear combination of rows chosen in constructing the trial wave function. This freedom can be exploited to improve the weak variational principle.

The d_r functions $\Phi_{T,l}^r(\mathbf{R})$ ($l = 1, 2, \dots, d_r$) are a basis for the irreducible representation $\Gamma_{\mathcal{G}}^r$ of \mathcal{G} , and hence transform into linear combinations of each other under all coordinate transformations $\mathcal{T} \in \mathcal{G}$. This implies that they also transform into linear combinations of each other under all coordinate transformations $\mathcal{T} \in \mathcal{G}_s$, where \mathcal{G}_s is any proper subgroup of \mathcal{G} . The subset of the matrices $\Gamma_{\mathcal{G}}^r(\mathcal{T})$ for which $\mathcal{T} \in \mathcal{G}_s$ is therefore a representation of \mathcal{G}_s . This representation is not in general irreducible.

To enumerate the different possibilities, begin by determining all the proper subgroups \mathcal{G}_s of \mathcal{G} . For each such subgroup, consider the representation of \mathcal{G}_s consisting of the matrices $\Gamma_{\mathcal{G}}^r(\mathcal{T})$ with $\mathcal{T} \in \mathcal{G}_s$. This representation may be decomposed into its irreducible components with respect to \mathcal{G}_s ,

$$\Gamma_{\mathcal{G}}^r = n_{q_1} \Gamma_{\mathcal{G}_s}^{q_1} \oplus n_{q_2} \Gamma_{\mathcal{G}_s}^{q_2} \oplus \dots \oplus n_{q_m} \Gamma_{\mathcal{G}_s}^{q_m}, \quad (19)$$

where the positive integer n_{q_i} is the number of times the irreducible representation $\Gamma_{\mathcal{G}_s}^{q_i}$ of \mathcal{G}_s appears, so $d_r = \sum_i n_{q_i} d_{q_i}$. The irreducible representations of \mathcal{G}_s appearing in Eq. (19) are said to be compatible¹⁴ with $\Gamma_{\mathcal{G}}^r$. Note that since the group containing only the identity element is always a subgroup of \mathcal{G} , it is always possible to find at least one subgroup for which the reduction of $\Gamma_{\mathcal{G}}^r$ contains a one-dimensional irreducible representation $\Gamma_{\mathcal{G}_s}^{q_i}$.

A trial function transforming as the l th row of $\Gamma_{\mathcal{G}}^r$ may contain components along all the compatible representations of \mathcal{G}_s , but it is always possible to construct linear combinations,

$$\Phi_{\text{T}}^{q_i}(\mathbf{R}) = \sum_{l=1}^{d_r} c_l^{q_i} \Phi_{T,l}^r(\mathbf{R}), \quad (20)$$

transforming according to each particular compatible representation $\Gamma_{\mathcal{G}_s}^{q_i}$. Every real function $\Phi_{\text{T}}^{q_i}(\mathbf{R})$ corresponding to a one-dimensional representation of \mathcal{G}_s has an invariant nodal surface with respect to \mathcal{G}_s . A DMC energy calculated using the nodes of such a function therefore satisfies the variational principle $E_{\text{DMC}} \geq E_0^{q_i}$.

Clearly, the strength of the variational principle obtained depends on the choices of the subgroup \mathcal{G}_s and the one-dimensional representation $\Gamma_{\mathcal{G}_s}^{q_i}$. In some cases, one can find a subgroup \mathcal{G}_s with a one-dimensional representation $\Gamma_{\mathcal{G}_s}^{q_i}$ which is compatible with $\Gamma_{\mathcal{G}}^r$ but incompatible with all those irreducible representations $\Gamma_{\mathcal{G}}^{r'}$ for which $E_0^{r'} < E_0^r$. A DMC energy calculated using the trial function $\Phi_{\text{T}}^{q_i}(\mathbf{R})$ is then guaranteed to be greater than or equal to E_0^r . In general, if one knows the ordering of the energy levels beforehand, one can use the compatibility analysis to find the one-dimensional irreducible representation $\Gamma_{\mathcal{G}_s}^{q_i}$ which gives the most stringent energy bound for the eigenvalue of interest.

As an application of this symmetry-constrained variational principle, consider a crystal with space group \mathcal{G} . We wish to establish whether it is possible to use fixed-node DMC to obtain a variational estimate of the eigenvalue $E_0(\mathbf{k})$ of the lowest energy eigenstate with crystal momentum \mathbf{k} . The relevant subgroup \mathcal{G}_s is the translation group, which is Abelian and has only one-dimensional irreducible representations. These are labeled by the crystal momentum \mathbf{k} , and so the statement of the symmetry-constrained variational principle is very straightforward: if the DMC trial function has crystal momentum \mathbf{k} , the DMC energy is greater than or equal to $E_0(\mathbf{k})$. It is worth noting that this statement holds whether or not the lowest energy state of crystal momentum \mathbf{k} is degenerate. In the degenerate case the trial function transforms according to a multi-dimensional irreducible representation of \mathcal{G} , but it still has crystal momentum \mathbf{k} and so still transforms according to a one-dimensional irreducible representation of the translation subgroup \mathcal{G}_s . This is sufficient to guarantee that the DMC energy is greater than or equal to $E_0(\mathbf{k})$.

The symmetry-constrained DMC variational principle for the lowest energy state of crystal momentum \mathbf{k} is unfortunately much less useful than it appears, because most Bloch states are complex and cannot be used as fixed-node DMC trial functions. Instead, the standard approach is to use a real linear combination of a Bloch function and its complex conjugate. (This is justified by the assumption of time-reversal invariance, which guarantees that if $\Psi_{\mathbf{k}}$ is an eigenfunction with eigenvalue $E_0(\mathbf{k})$ then so is $\Psi_{\mathbf{k}}^*$.) Since such trial functions contain components with two different wave vectors, \mathbf{k} and $-\mathbf{k}$, they do not transform according to a single irreducible representation of the translation group. The symmetry-constrained variational theorem is therefore inapplicable, and it is possible that the DMC energy may lie below $E_0(\mathbf{k})$. In Sec. VIII we show by means of a specific example that such calculations may indeed produce a DMC energy which is lower than $E_0(\mathbf{k})$.

An important exception arises when the wave vector \mathbf{k} is equal to half a reciprocal lattice vector, in which case \mathbf{k} and $-\mathbf{k}$ are alternative labels for the same irreducible representation of the translation group. The linear combination of $\Psi_{\mathbf{k}}$ and $\Psi_{\mathbf{k}}^*$ is then a pure Bloch function, and the normal proof of the symmetry-constrained variational principle applies. As long as \mathbf{k} equals half a reciprocal lattice vector, the DMC energy is greater than or equal to the energy of the lowest exact eigenstate with crystal momentum \mathbf{k} .

VI. GENERALIZATIONS OF THE TILING THEOREM

In his paper on fermion nodes,⁸ Ceperley stated that the tiling theorem could be generalized to the case where there were other discrete symmetries present. A more precise statement is that, given a Hamiltonian with a reasonable local potential and a symmetry group \mathcal{G} , the tiling theorem applies to any real state which is the lowest energy eigenfunction of a symmetry $\Gamma_{\mathcal{G}}^r$ with dimension $d_r = 1$. This can be demonstrated via a simple generalization of Ceperley's proof⁸ of the ground-state tiling theorem.

Consider the real antisymmetric state $\Psi_0^r(\mathbf{R})$ which is the lowest energy eigenfunction transforming according to the one-dimensional irreducible representation $\Gamma_{\mathcal{G}}^r$. This function may have many nodal pockets, but pick one at random and color it blue. Now apply a symmetry operator from the group containing the spatial symmetries (rotations, translations, reflections and inversions) and the permutations. Since the nodal surface is invariant, this symmetry operator maps the region of space within the blue nodal pocket into itself or into one of the other nodal pockets. If the blue pocket is mapped into some other nodal pocket, this pocket is equivalent to the blue one by symmetry and is also colored blue. Repeat this process for every operator in the group, until all the

pockets equivalent to the original one have been found and colored blue.

There are now two possibilities: the blue regions may fill the entire configuration space, in which case the nodal pockets are all equivalent by symmetry and the tiling theorem holds; or there may be other inequivalent nodal pockets which have not yet been found. We can rule out the second possibility using the following argument.

Assume that the blue nodal pockets do not fill the configuration space, and that the local potential $V(\mathbf{R})$ and all its derivatives are finite except at the Coulomb singularities occurring when two charged particles approach each other. As long as the system is not one-dimensional (in which case different arguments are required), this ensures that almost every point on the nodal surface lies a finite distance away from the nearest singularity in the potential. The eigenfunction $\Psi_0^r(\mathbf{R})$ may therefore be expanded as a power series with a finite radius of convergence about almost any point \mathbf{R}_s on the nodal surface. If the gradient of $\Psi_0^r(\mathbf{R})$ is assumed to be zero over any finite area of the nodal surface surrounding \mathbf{R}_s , it can be shown that every term in this series has to be zero, and hence that $\Psi_0^r(\mathbf{R}) = 0$ everywhere within the radius of convergence. Since any solution of the Schrödinger equation can be analytically continued around the isolated singularities in the potential, this further implies that $\Psi_0^r(\mathbf{R})$ is zero everywhere. We therefore conclude that the gradient of $\Psi_0^r(\mathbf{R})$ must be non-zero almost everywhere on the nodal surface.

Now consider the trial function $\tilde{\Psi}^r(\mathbf{R})$, which is defined to equal $\Psi_0^r(\mathbf{R})$ within the blue pockets and zero elsewhere. This trial function is antisymmetric and transforms according to the irreducible representation $\Gamma_{\mathcal{G}}^r$, but has gradient discontinuities on the nodal surfaces separating the blue pockets from the rest of configuration space. It satisfies the Schrödinger-like equation,

$$\hat{H}\tilde{\Psi}^r(\mathbf{R}) = E_0^r\tilde{\Psi}^r(\mathbf{R}) + \delta^r, \quad (21)$$

where the symbol δ^r denotes the delta functions produced by the action of the kinetic energy operator on the gradient discontinuities. The delta functions occur where $\tilde{\Psi}^r = 0$ and so do not affect the energy expectation value,

$$E_0^r = \frac{\langle \Psi_0^r | \hat{H} | \Psi_0^r \rangle}{\langle \Psi_0^r | \Psi_0^r \rangle} = \frac{\langle \tilde{\Psi}^r | \hat{H} | \tilde{\Psi}^r \rangle}{\langle \tilde{\Psi}^r | \tilde{\Psi}^r \rangle}. \quad (22)$$

We know, however, that a state which has gradient discontinuities almost everywhere on a finite area of the nodal surface cannot be an eigenfunction unless the potential is infinite almost everywhere on that area. Since we are assuming that this is not the case, the function $\tilde{\Psi}^r$ must contain excited-state components of symmetry $\Gamma_{\mathcal{G}}^r$ and cannot have the same energy expectation value as the lowest energy state of that symmetry. This conclusion contradicts Eq. (22), and so the assumption that the blue nodal pockets do not fill the configuration space must have been incorrect. All the nodal pockets of Ψ_0^r are therefore equivalent by symmetry.

This proves the tiling theorem for any real state which is the lowest energy eigenfunction of a symmetry $\Gamma_{\mathcal{G}}^r$ with dimension $d_r = 1$. An obvious corollary is that there is also a tiling theorem for the lowest energy state transforming according to any one-dimensional irreducible representation of any subgroup \mathcal{G}_s of \mathcal{G} . This statement is analogous to the weaker variational principle discussed in Sec. V. In every case when we have demonstrated the existence of a DMC variational principle, we have therefore also been able to demonstrate the existence of a tiling theorem. Our analysis has been restricted to the physically interesting case of a local potential which is finite everywhere except at Coulomb singularities, but our conclusions may be somewhat more general than this suggests.

The familiar many-fermion ground-state tiling theorem may be viewed as a special case of the subgroup tiling theorem mentioned above. The permutation group is always a subgroup of the full symmetry group (which contains both spatial and permutation symmetries), and the many-fermion ground state is the lowest energy state which transforms according to the one-dimensional antisymmetric irreducible representation of that subgroup. The subgroup tiling theorem therefore guarantees that the many-fermion ground state possesses the tiling property. Note that the tiling property holds with respect to the permutation subgroup, not the full symmetry group. This means that it is only the elements of the permutation subgroup that need be applied to the initial blue pocket to find all equivalent pockets and turn the whole configuration space blue.

The above derivation of the subgroup tiling theorem only applies to states that transform according to one-dimensional irreducible representations of the chosen subgroup \mathcal{G}_s . Such states may also transform according to multi-dimensional irreducible representations of the full symmetry group \mathcal{G} , so the tiling theorem is not restricted to non-degenerate energy levels. In systems with degenerate many-fermion ground states, for example, any real linear combination of the degenerate ground states is antisymmetric and so possesses the tiling property with respect to the permutation subgroup. This result holds even though the nodal surface is not invariant under all the operators from the full symmetry group.

The most important consequence of the generalized tiling theorem is exactly as in the ground-state case. It is common for a fixed-node DMC trial wave function to have the same nodal surface as an energy eigenfunction calculated using an approximate method such as local-density-functional theory. The approximate Hamiltonian is chosen to have the same symmetries as the exact Hamiltonian, but may also have extra symmetries which are not relevant to the argument and may be ignored. If the approximate Hamiltonian has a reasonably well behaved local potential, its eigenstates have the same tiling properties with respect to \mathcal{G} as the corresponding exact eigenstates. The lowest energy eigenstate transforming according to any one-dimensional irreducible represen-

tation of \mathcal{G} or any subgroup of \mathcal{G} therefore satisfies the tiling theorem. This ensures that the energy produced by a DMC simulation using the nodal surface of such a state is independent of the initial walker distribution.

VII. TIGHT-BINDING EXAMPLE

This section and the next describe simple examples that show what happens when a trial wave function transforming according to an irreducible representation with $d_r > 1$ is used to define the trial nodal surface for a DMC simulation. We find that the DMC energy may indeed be lower than the eigenvalue of the lowest exact eigenstate with the same symmetry as the trial function. This demonstrates that the variational principle of Eq. (17) does not apply when $d_r > 1$.

In searching for a suitable example system, we found it convenient to impose the following restrictions: (i) the group of the Hamiltonian is finite; (ii) the trial wave function and its nodal surface can be easily visualized; and (iii) the exact eigenstates of the Hamiltonian and the pocket ground states of Eq. (9) can be calculated without numerical error. These restrictions are unnecessary, but make the analysis much simpler. To satisfy criterion (ii), we must choose a system containing at most three electrons in one dimension or a single electron in two or three dimensions. The nodal surfaces of one-dimensional systems are not easily altered because they are almost entirely determined by the antisymmetry of the wave function, so we decided to concentrate on one-electron systems in two and three spatial dimensions.

The first system we studied was an electron confined to a rectangular box in two or three dimensions. Although this system does have multi-dimensional irreducible representations, we failed to find an example in which the DMC energy calculated using a trial state of a given symmetry was less than the eigenvalue of the lowest energy eigenstate of that symmetry. The second system we tried was more successful. We start by discussing a simple tight-binding realization of this system, and then in Sec. VIII present an alternative realization based on a separable solution of the Schrödinger equation.

Consider a molecule containing one electron moving in the potential of three protons fixed at the corners of an equilateral triangle. The symmetry group of the Hamiltonian of this system is called D_{3h} .¹⁴ A convenient way to generate DMC trial wave functions with specific symmetries is to solve the Schrödinger equation within a tight-binding approximation using a single spherically-symmetric atomic-like orbital $\xi(\mathbf{r}|)$ centered on each proton. Once a tight-binding eigenfunction has been found and used to define a trial nodal surface, the fixed-node DMC algorithm can be used to solve the original Hamiltonian exactly subject to the fixed-node constraint.

The ground state of the molecule is a non-degenerate nodeless function transforming according to the identity

representation. Some of the excited-state eigenfunctions must be doubly degenerate, however, since the symmetry group D_{3h} has two two-dimensional irreducible representations, one of which is called $\Gamma_{D_{3h}}^3$.

The tight-binding Hamiltonian has only three eigenstates, the nodeless ground state and a degenerate pair of excited states which can be written as the Bloch functions,

$$\begin{aligned}\Psi_+(\mathbf{r}) &= \sum_{j=0}^2 \xi(|\mathbf{r} - \mathbf{d}_j|) e^{i2\pi j/3}, \\ \Psi_-(\mathbf{r}) &= \sum_{j=0}^2 \xi(|\mathbf{r} - \mathbf{d}_j|) e^{-i2\pi j/3},\end{aligned}\quad (23)$$

where \mathbf{d}_0 , \mathbf{d}_1 , and \mathbf{d}_2 are the position vectors of the three protons. These two Bloch functions transform into linear combinations of each other under the operations of the point group (there is no need to include time-reversal symmetry) and form a basis for $\Gamma_{D_{3h}}^3$. Taking linear combinations of Ψ_+ and Ψ_- , one can form the real functions,

$$\begin{aligned}\Psi_1(\mathbf{r}) &= \xi(|\mathbf{r} - \mathbf{d}_1|) - \xi(|\mathbf{r} - \mathbf{d}_2|), \\ \Psi_2(\mathbf{r}) &= 2\xi(|\mathbf{r} - \mathbf{d}_0|) - \xi(|\mathbf{r} - \mathbf{d}_1|) - \xi(|\mathbf{r} - \mathbf{d}_2|),\end{aligned}\quad (24)$$

which form an alternative basis for the same irreducible representation.

Fig. (1) shows the nodal surfaces of Ψ_1 and Ψ_2 along with the expansion coefficients from Eq. (24). The nodal surface of Ψ_1 does not depend on the particular spherically-symmetric tight-binding basis functions chosen and turns out to be an exact excited-state nodal surface. The nodal surface of Ψ_2 is not exact, however, and its precise shape depends on the details of the atomic-like orbitals used in the tight-binding model. Different choices of $\xi(|\mathbf{r}|)$ give trial functions with the same symmetries but different nodal surfaces. By changing $\xi(|\mathbf{r}|)$, it is possible to change the relative sizes of the two nodal pockets of Ψ_2 , causing one to grow at the expense of the other. As in the example of the 2s state of the H atom discussed earlier, this suggests that in many cases the pocket eigenvalue of one of the two nodal pockets will be too high while that of the other is too low. The DMC energy will then lie below the energy of the exact eigenstate of interest. In Sec. VIII we numerically solve a specific example with the same symmetry properties as this system and observe exactly this behavior.

Here we apply the weaker variational principle described in the previous section to the degenerate excited state with symmetry $\Gamma_{D_{3h}}^3$ of the group D_{3h} . The largest subgroups C_{3h} and D_3 each have six elements. If the subgroup D_3 is used, the compatibility relation of Eq. (19) becomes,

$$\Gamma_{D_{3h}}^3 = \Gamma_{D_3}^3, \quad (25)$$

where $\Gamma_{D_3}^3$ is two dimensional. This result is not useful since we are seeking a reduction that contains one-dimensional representations. Using the subgroup C_{3h} results in two one-dimensional representations

$$\Gamma_{D_{3h}}^3 = \Gamma_{C_{3h}}^5 \oplus \Gamma_{C_{3h}}^6. \quad (26)$$

However, any trial wave function that transforms as either $\Gamma_{C_{3h}}^5$ or $\Gamma_{C_{3h}}^6$ is complex and therefore unsuitable for fixed-node DMC.

If we use the smaller subgroup, C_{2v} , which has four elements, we obtain the compatibility relation

$$\Gamma_{D_{3h}}^3 = \Gamma_{C_{2v}}^1 \oplus \Gamma_{C_{2v}}^4, \quad (27)$$

from which we can construct real trial wave functions and apply the weaker variational principle. In fact, the trial functions Ψ_1 and Ψ_2 already have the correct transformation properties: Ψ_1 transforms as the one-dimensional representation $\Gamma_{C_{2v}}^4$, while Ψ_2 transforms as the one-dimensional representation $\Gamma_{C_{2v}}^1$. The group C_{2v} therefore preserves the nodal surfaces of Ψ_1 and Ψ_2 . Because the symmetry corresponding to the representation $\Gamma_{C_{2v}}^1$ is compatible with the ground-state symmetry as well as with $\Gamma_{D_{3h}}^3$, a DMC simulation using the trial function Ψ_2 satisfies only the weaker variational principle $E_{\text{DMC}} \geq E_0$, where E_0 is the overall ground-state energy. The representation $\Gamma_{C_{2v}}^4$ is not compatible with the ground-state symmetry, however, and so a simulation using the trial function Ψ_1 gives a stronger variational principle. For the example studied in the next section, it turns out that the $\Gamma_{D_{3h}}^3$ state of interest is the lowest energy exact eigenstate with which the representation $\Gamma_{C_{2v}}^4$ is compatible. The strong variational principle therefore applies and $E_{\text{DMC}} \geq E_0^3$, where E_0^3 is the exact $\Gamma_{D_{3h}}^3$ eigenvalue. It is important to appreciate that this is not a general result; it is not always possible to pick a trial function that maintains the strong variational principle for a given symmetry.

Note that the strong variational principle applies because the trial wave function Ψ_1 transforms according to the irreducible representation $\Gamma_{C_{2v}}^4$ of the subgroup C_{2v} . If we had chosen a different pair of trial functions, constructed by taking linear combinations of Ψ_1 and Ψ_2 , both would have contained components along $\Gamma_{C_{2v}}^4$ and $\Gamma_{C_{2v}}^1$. The only subgroup preserving the nodes would then have been the group of the identity, and the only variational principle would have been with respect to the overall ground-state energy, $E_{\text{DMC}} \geq E_0$. This illustrates the general rule that the strongest variational principles are obtained by choosing trial functions which transform according to specific one-dimensional irreducible representations of specific subgroups of \mathcal{G} .

VIII. SEPARABLE EXAMPLE

We now present an explicit solution of a different example with the same D_{3h} symmetry group as the triangular molecule discussed above. Consider a particle of unit mass moving in a triangular potential in three dimensions. The wave function $\Psi(\mathbf{r})$ obeys the Schrödinger equation,

$$\left(-\frac{1}{2}\nabla^2 + V(\mathbf{r})\right)\Psi(\mathbf{r}) = E\Psi(\mathbf{r}), \quad (28)$$

where

$$V(\mathbf{r}) = \frac{\cos(3\theta)}{\rho^2}, \quad (29)$$

with ρ , θ and z the usual cylindrical coordinates. The boundary conditions are $\Psi(\rho, \theta, z) = 0$ for $\rho \geq 1$ or $|z| \geq \pi/2$, confining the particle within a cylinder.

Writing $\Psi(\mathbf{r}) = R(\rho)\Theta(\theta)Z(z)$, the Schrödinger equation separates into:

$$-\frac{1}{2}\frac{d^2Z}{dz^2} = E_z Z, \quad (30)$$

$$-\frac{1}{2}\frac{d^2\Theta}{d\theta^2} + \cos(3\theta)\Theta = E_\theta\Theta, \quad (31)$$

$$-\frac{1}{2\rho}\frac{d}{d\rho}\left(\rho\frac{dR}{d\rho}\right) + \left(E_z + \frac{E_\theta}{\rho^2}\right)R = ER. \quad (32)$$

The lowest energy eigenfunction of Eq. (30) is

$$Z(z) = \sqrt{\frac{2}{\pi}}\cos(z), \quad (33)$$

with eigenvalue $E_z = 1/2$. Eq. (32) may be simplified by the substitutions $r = \sqrt{2(E - E_z)}\rho$ and $\nu = \sqrt{2E_\theta}$, which yield Bessel's equation,

$$r^2\frac{dR}{dr^2} + r\frac{dR}{dr} + (r^2 - \nu^2)R = 0. \quad (34)$$

The general solutions are the Bessel and Neumann functions, $J_\nu(r)$ and $N_\nu(r)$, but only $J_\nu(r)$ is well behaved at the origin. Hence

$$R(\rho) = J_{\sqrt{2E_\theta}}\left(\sqrt{2(E - E_z)}\rho\right), \quad (35)$$

with the energy E determined by the boundary condition at $\rho = 1$,

$$J_{\sqrt{2E_\theta}}(\sqrt{2(E - E_z)}) = 0. \quad (36)$$

Eq. (31) can be transformed into Mathieu's equation¹⁵ by a simple change of variables, but here we solve it numerically by expanding the eigenfunctions in (normalized) sines and cosines,

$$\Theta(\theta) = a_0\frac{1}{\sqrt{2\pi}} + \sum_{n=1}^M\left(a_n\frac{\cos(n\theta)}{\sqrt{\pi}} + b_n\frac{\sin(n\theta)}{\sqrt{\pi}}\right), \quad (37)$$

and diagonalizing the corresponding Hamiltonian matrix. The results converge rapidly with M , and choosing $M = 50$ gives very accurate eigenvalues for the lowest few eigenstates.

The three lowest energy angular eigenfunctions are shown in Fig. (2). As stated in Sec. VII, the lowest energy eigenstate is a nodeless function invariant under

all elements of the symmetry group of the Hamiltonian. The next two states are a degenerate pair forming a basis for the irreducible representation $\Gamma_{D_{3h}}^3$. One of the two has nodes at $\theta = 0$ and $\theta = \pi$, and will be called Ψ_1 in analogy with the corresponding state from Sec. VII; the other has nodes at $\theta = \pm 1.7934$ radians, and will be called Ψ_2 . Note that Ψ_1 is the lowest energy eigenfunction transforming according to the one-dimensional irreducible representation $\Gamma_{C_{2v}}^4$ of the subgroup C_{2v} ; it therefore possesses the tiling property with respect to C_{2v} . The $\Gamma_{C_{2v}}^1$ symmetry of Ψ_2 is shared by the overall ground state, however, so Ψ_2 is not the lowest eigenstate of that subgroup symmetry and does not satisfy a tiling theorem.

Consider how DMC might be used to find the eigenvalue of the lowest energy $\Gamma_{D_{3h}}^3$ doublet. We do not want to impose the exact nodal surface since DMC would then give the exact answer and we would learn little about variational principles, so we seek a trial function with a different nodal surface but the same symmetry. We choose to generate such a trial function by solving the Schrödinger equation for a different triangular potential,

$$\hat{H} = -\frac{1}{2}\nabla^2 + \frac{\cos(3\theta)}{\rho^2} + \mu\frac{\cos(6\theta)}{\rho^2}, \quad (38)$$

where μ is an adjustable parameter. The first three angular eigenfunctions of this Hamiltonian when $\mu = 5$ are shown in Fig. (3). Since the $\cos(6\theta)$ term does not change the symmetry group, these eigenfunctions still belong to the same irreducible representations. However, the nodal angle of Ψ_2 has moved slightly in response to the perturbation. One of the two nodal volumes of this trial wave function is therefore slightly too small, while the other is slightly too large.

The trial nodal pocket that is too large (small) encloses (is enclosed by) the corresponding exact nodal pocket. We can therefore apply the variational argument used in the discussion of the 2s state of the hydrogen atom to show that the pocket eigenvalue from the pocket that is too small must be greater than the exact eigenvalue, while the pocket eigenvalue from the pocket that is too large must be less than the exact eigenvalue. As in the H 2s example, therefore, the DMC energy is always \leq the exact eigenvalue. The maximum of the DMC energy, equal to the exact $\Gamma_{D_{3h}}^3$ ground-state eigenvalue, is attained only when the nodal angle is exact; and the slope of the graph of DMC energy against nodal angle changes discontinuously at this point. The error in the DMC energy is first order, not second order, in the error in the nodal angle.

This analysis is confirmed by the results of a full calculation given in Fig. (4), which shows how the angular pocket eigenvalues E_θ of the two pockets depend on the angular half width of the nodal pocket centered on $\theta = 0$. As expected, E_θ is too large when the nodal pocket is too small and vice-versa. Fig. (5) shows the dependence of the total pocket eigenvalues E on the angular half width

of the nodal pocket centered on $\theta = 0$, confirming that an increase in angular half width gives rise to a decrease in total eigenvalue and vice-versa. The numerical results therefore support the conclusions of the variational argument.

Note, finally, that Eq. (31) can be interpreted as the Schrödinger equation for a one-dimensional crystal with periodic boundary conditions, in which case Ψ_1 and Ψ_2 are real linear combinations of Bloch waves with equal and opposite crystal momenta. Seen from this viewpoint, the degeneracy of Ψ_1 and Ψ_2 arises from the time-reversal (complex-conjugation) symmetry of the real Hamiltonian rather than from its spatial symmetry, but the failure of the symmetry-constrained variational principle is still apparent. This confirms the assertion made in Sec. V: a DMC simulation using a real trial state constructed from Bloch states with equal and opposite crystal momenta may yield an energy below that of the lowest exact eigenstate with that crystal momentum.

IX. CONCLUSIONS

The main lesson to be learned from this work is that symmetry arguments cannot be applied to fixed-node DMC unless the symmetries of both the Hamiltonian and the nodal surface of the trial wave function are taken into account. The fixed-node DMC algorithm solves the Hamiltonian subject to the boundary conditions imposed by the trial nodal surface, and so the relevant symmetry group \mathcal{G}_{FN} contains only those symmetry operations that leave both the Hamiltonian and the trial nodal surface (boundary conditions) invariant. This “group of the fixed-node Hamiltonian” is a subgroup of the more familiar “group of the Hamiltonian”, \mathcal{G} .

If the trial function transforms according to a real one-dimensional irreducible representation Γ^r of \mathcal{G} , all symmetry operations in \mathcal{G} simply multiply the trial function by a real number. This does not change the nodal surface and hence $\mathcal{G} = \mathcal{G}_{\text{FN}}$. The symmetry-constrained variational principle then implies: (i) that the fixed-node DMC energy is greater than or equal to the eigenvalue of the lowest energy exact eigenstate that transforms according to the same one-dimensional irreducible representation as the trial state; and (ii) that the error in the DMC energy is in general second order in the difference between the nodal surfaces of the lowest energy exact eigenstate that transforms as Γ^r and the trial function.

If the irreducible representation to which the trial function belongs is of dimension greater than one, it is inevitable that some of the symmetry operations from \mathcal{G} will change the trial nodal surface. The nodal surfaces of the states Ψ_1 and Ψ_2 shown in Fig. (1) are examples of this. The symmetry-constrained variational principle need not apply in such cases, because the symmetrized state $\bar{\Psi}_\alpha^r$ used in its derivation need not be zero everywhere on the trial nodal surface. The delta functions

produced when the kinetic energy operator is applied to the fixed-node pocket ground state ϕ_α from Eq. (9) may therefore contribute to the expectation value in Eq. (17).

In such cases, a weaker version of the symmetry-constrained variational principle can be obtained by re-analyzing the problem using only the symmetries in the subgroup \mathcal{G}_{FN} . The idea is to forget all the symmetry operations which change the nodes of the trial function, and consider only those which leave the trial nodal surface invariant. The symmetry-constrained variational principle then applies as long as the symmetries are labeled using the irreducible representations of \mathcal{G}_{FN} .

In summary, a useful DMC variational principle exists whenever the trial state transforms according to a one-dimensional irreducible representation Γ^r of \mathcal{G} or any subgroup of \mathcal{G} . In many DMC simulations, the nodal surface of the trial state is the same as that of an eigenstate of an approximate Hamiltonian such as the local-density-functional Hamiltonian. If the state used to define the nodal surface is the lowest energy eigenstate with symmetry Γ^r of an approximate Hamiltonian with a reasonable local potential, the generalized tiling theorem discussed in Sec. VI shows that all the nodal pockets are equivalent by symmetry. The DMC energy is therefore independent of the initial distribution of walkers among the nodal pockets.

The ordinary fixed-node approximation provides a good example of these ideas. The many-electron ground state is never the overall ground state (which is bosonic), and may be degenerate, in which case we cannot prove the existence of a variational principle by analyzing the problem using the full symmetry group. We can, however, use the permutation group, which is always a subgroup of the full symmetry group. The many-electron trial function transforms according to the one-dimensional antisymmetric irreducible representation of this subgroup. The weaker variational principle therefore guarantees that the fixed-node DMC energy is greater than or equal to the energy of the many-electron ground state; and the generalized tiling theorem guarantees that the exact many-electron ground state possesses the tiling property with respect to permutations. This shows that the ground-state versions of the fixed-node variational principle¹⁰ and tiling theorem⁸ may be regarded as special cases of the more general versions discussed in this paper.

The different members of a set of trial functions forming a basis for a multi-dimensional irreducible representation of \mathcal{G} have different nodal surfaces and need not all produce the same fixed-node DMC energy. The strength of the weaker variational principle may therefore be optimized by using specific linear combinations of these basis functions. The best linear combinations transform according to one-dimensional irreducible representations of subgroups of \mathcal{G} , and may be found following the procedure explained in Sec. V. If this procedure is not carried out, trial functions belonging to multi-dimensional irreducible representations of \mathcal{G} usually have nodal surfaces

with very little spatial symmetry. In many cases, the only symmetry operations that leave the nodal surface invariant are the elements of the permutation group, and the only variational principle that survives is the one relating to the many-electron ground state.

X. ACKNOWLEDGEMENTS

We thank the Engineering and Physical Sciences Research Council, UK, for financial support under grants GR/L40113 and GR/M05348.

-
- * Present address: Lawrence Livermore National Laboratory, Livermore, CA 94550, USA.
- ¹ D. Ceperley, G. Chester, and M. Kalos, *Phys. Rev. B* **16**, 3081, (1971).
 - ² B. L. Hammond, W. A. Lester, Jr., and P. J. Reynolds, *Monte Carlo Methods in Ab Initio Quantum Chemistry*, (World Scientific, Singapore, 1994).
 - ³ J. B. Anderson, *J. Chem. Phys.* **65**, 4121, (1976).
 - ⁴ R. M. Grimes, B. L. Hammond, P. J. Reynolds, and W. A. Lester, Jr., *J. Chem. Phys.* **85**, 4749, (1986).
 - ⁵ L. Mitáš, *Comput. Phys. Commun.* **96**, 107, (1996).
 - ⁶ L. Mitáš, *Electronic Properties of Solids Using Cluster Methods*, eds. T. A. Kaplan and S. D. Mahanti (Plenum, New York, 1995), p151.
 - ⁷ A. J. Williamson, R. Q. Hood, R. J. Needs, and G. Rajagopal, *Phys. Rev. B* **57**, 12140, (1998).
 - ⁸ D. Ceperley, *J. Stat. Phys.* **63**, 1237 (1991).
 - ⁹ G. Ortiz, D. M. Ceperley, and R. M. Martin, *Phys. Rev. Lett.* **71**, 2777 (1993).
 - ¹⁰ P. J. Reynolds, D. M. Ceperley, B. J. Alder, and W. A. Lester, Jr., *J. Chem. Phys.* **77**, 5593 (1982).
 - ¹¹ J. W. Moskowitz, K. E. Schmidt, M. A. Lee, and M. H. Kalos, *J. Chem. Phys.* **77**, 343 (1982).
 - ¹² The results presented in this section also hold for infinite order compact Lie groups, and hence are sufficiently general to encompass most fixed-node DMC simulations of real electronic systems.
 - ¹³ M. Caffarel and P. Claverie, *J. Chem. Phys.* **88**, 1100 (1987).
 - ¹⁴ J. F. Cornwell, *Group Theory in Physics*, (Academic Press, London, 1984), Vol. 1.
 - ¹⁵ See, for example, *Handbook of Mathematical Functions*, eds. M. Abramowitz and I. A. Stegun (Dover, New York, 1972), p722.

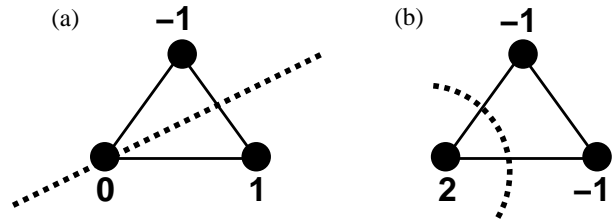


FIG. 1. The single-electron trial states (a) Ψ_1 and (b) Ψ_2 from Eq. (24). The dashed lines show where the nodal surfaces cross the plane of the molecule. The expansion coefficients of Ψ_1 and Ψ_2 in terms of the tight-binding basis functions are also shown.

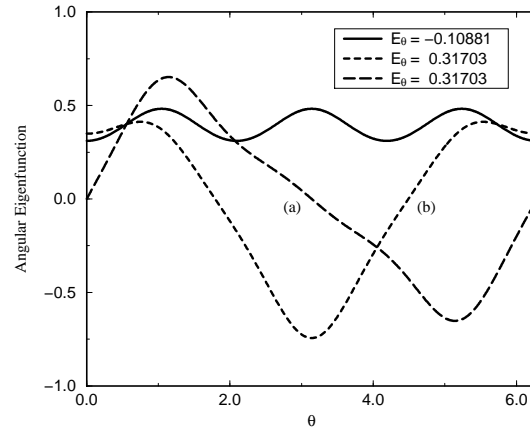


FIG. 2. Angular eigenfunctions $\Theta(\theta)$ of the separable Hamiltonian of Eq. (28) with $V(\mathbf{r}) = \cos(3\theta)/\rho^2$. The functions (a) and (b) are analogous to the tight-binding states (a) and (b) shown in Fig. (1). The corresponding angular eigenvalues E_θ are also shown.

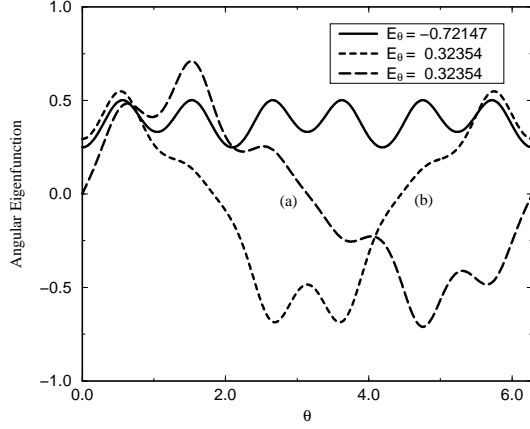


FIG. 3. Angular eigenfunctions $\Theta(\theta)$ of the separable Hamiltonian of Eq. (28) with $V(\mathbf{r}) = (\cos(3\theta) + 5 \cos(6\theta))/\rho^2$. The functions (a) and (b) are analogous to the tight-binding states (a) and (b) shown in Fig. (1). The corresponding angular eigenvalues E_θ are also shown.

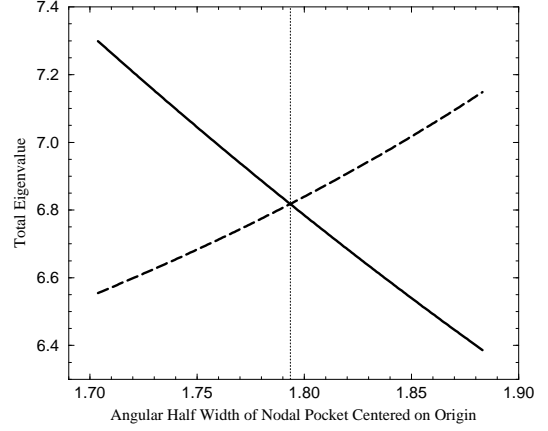


FIG. 5. The total pocket eigenvalues E of the two nodal pockets of the separable example from Sec. VIII. The Hamiltonian is that of Eq. (28) with $V(\mathbf{r}) = \cos(3\theta)/\rho^2$, and the eigenvalues are plotted as functions of the angular half width of the nodal pocket centered on $\theta = 0$. The vertical line shows the nodal surface of the exact excited state Ψ_2 .

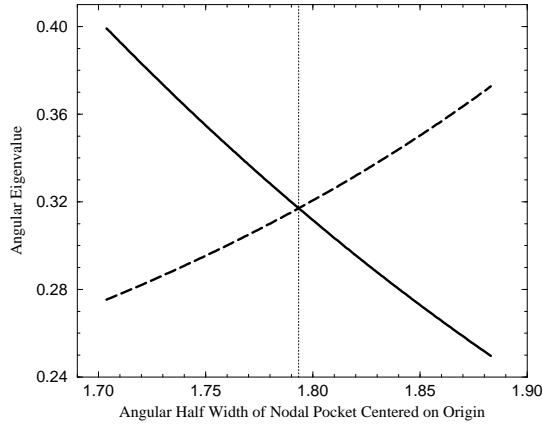


FIG. 4. The angular pocket eigenvalues E_θ of the two nodal pockets of the separable example from Sec. VIII. The Hamiltonian is that of Eq. (28) with $V(\mathbf{r}) = \cos(3\theta)/\rho^2$, and the eigenvalues are plotted as functions of the angular half width of the nodal pocket centered on $\theta = 0$. The vertical line shows the nodal surface of the exact excited state Ψ_2 .